MODELLING OF SOLIDIFICATION OF POROUS METAL-HYDROGEN ALLOYS

By

Yu Zheng

MSc Thesis

May 12, 1995

Submitted to the Department of
Materials Science and Engineering in Partial Fulfillment
of the Requirements for the Degree of

Master of Science in
Materials Science and Engineering
at the
Massachusetts Institute of Technology
June 1995

Signature of Author: _____
Department of Materials Science and Engineering
May 12, 1995

Certified by: _____
Kenneth C. Russell
Professor of Materials Science and Engineering
Thesis Supervisor

Accepted by: _____
Carl V. Thompson II
Professor of Electronic Materials
Chair, Departmental Committee on
Graduate Students

MODELLING OF SOLIDIFICATION OF POROUS METAL-HYDROGEN ALLOYS

by

Yu Zheng

Submitted to the Department of Materials Science and Engineering on May 12, 1995 in partial fulfillment of the requirements for the Degree of Master of Science in Materials Science and Engineering

ABSTRACT

Gas porosity usually weakens the properties of solidified metals by introducing cracks and other defects, therefore, is unwanted in the end products. However, when the gas porosity is carefully controlled in its size, geometry and distribution, the porous metals might have good properties as well as the advantage of low densities. A New method called GASAR has been developed in Dnepropetrovsk Metallurgical Institute in Ukraine for producing such materials with controlled porosity by directly solidifying solid-hydrogen eutectics under high pressure of hydrogen gas. The present work calculates the equilibrium phase diagrams of binary metal-hydrogen alloys. The effect of a third element on the phase diagram is also investigated. Then the steady-state eutectic growth of metal-hydrogen alloys is studied by applying the Jackson-Hunt's theory. Furthermore, after comparing the coupled eutectic growth with the dendrite growth of the primary metal phase, an eutectic stable region, or a coupled zone, is estimated and presented on the phase diagram.

Thesis Supervisor: Dr. K. C. Russell

Title: Professor of Materials Science and Engineering

1. INTRODUCTION

A novel method named GASAR was developed by the Dnepropetrovsk Metallurgical Institute (DMI) in Ukraine to produce porous materials[1]. By controlling the process variables such as pressure, cooling rate and direction, pores with desirable morphology, size, orientation and distribution can be created. Unlike conventional materials, the new product has high strength and rigidity, as well as the ability of allowing forming and shaping operations like welding, cutting, bending and machining.

Figure 1.1-1.2 are pictures of different porous structures which are obtained through the process with different process variables[2].

1.1 APPLICATIONS OF GASAR MATERIALS

Combining good mechanical or thermal properties with low densities, the GASAR materials have many applications. Some of them are listed as following:[1,2]

* Ni filters (Volgograd Chemical Factory), which possess a long working life and are easily cleaned by simple reversal of pressure.
* Insulin filters, GASAR Ni tubes function as supports for a covering organic layer to produce filters with pore sizes of 100-200 nm.
* Al-bronze and bronze bearings in food processing industry, which are fabricated from tubes with radially oriented pores.
* Ceramic catalyst supports for high temperature environments such as rocket and jet engines.
* Porous Mg light-weight panels for the space program.
* Oxygenators for water purification.

1.2 THE GASAR PROCESS

Under normal solidification conditions, most of the major metals used in the production of basic structural and tool materials(i.e. Fe, Ni, Al, Cu, Mg, Co, Mn, W, Cr, Mo, and Be) are not likely to form hydrides. A metal-hydrogen solution may be prepared by melting the various metals in an atmosphere containing hydrogen at certain pressure to give desired hydrogen concentration.

Then, the GASAR porous materials are obtained by solidifying the melts under directional heat removal at various rates and pressure. Referred to the phase diagram(Figure 1.3), the solidification process is a solid-gas eutectic reaction, $\text{Liquid} \rightarrow \text{Solid} + \text{Gas}$. Similar to traditional eutectic transformations, it is the coupled growth of two phases: a solid phase and a gas phase. Under different nucleation methods, solidification rate and hydrogen pressure, a wide range of structures of pores were observed. [1]

2. PHASE DIAGRAM OF BINARY METAL-HYDROGEN ALLOYS

To understand solidification, the phase diagram, or the distribution of phases at equilibrium over the range of temperature, composition and pressure, must be known. For a metal-hydrogen alloy, there are three primary phases: a liquid phase(the liquid metal with hydrogen dissolved in), a solid phase(the solid metal with hydrogen dissolved in) and a gas phase(the mixture of hydrogen gas with the metal's vapor). With respect to a fixed pressure but varying temperatures, according to the phase rule, only two of the three phases can coexist: liquid vs. gas, solid vs. liquid and solid vs. gas. Consequently, the task of illustrating the phase diagram is to find out the equilibrium boundaries of those phases. Generally, the gas phase is favored at very high temperature or close to pure hydrogen in composition, while the liquid is at medium temperature(between the melting point to the boiling point) and low composition of hydrogen, and the solid is at low temperature as well as low composition of H. Thus the phase diagram looks like Figure 2.1(not to scale).

2.1 LIQUID VS. GAS

At a medium temperature T_1, if the concentration of hydrogen is below the solubility of it in the liquid metal, or $C<C_1$, the whole metal-hydrogen system is in a pure liquid phase. If the composition of hydrogen is high enough that the boiling point at this composition is lower than T_1, or $C>C_2$, all of the metal will evaporate into the surrounding hydrogen gas, therefore, the system is in a pure gas phase. If the composition is in between, or $C_1<C<C_2$, the system is in a mixture of liquid phase and gas phase, where the composition of liquid is C_1 and the composition of gas is

C_2.

When T_1 varies, the solubility of hydrogen in the liquid metal forms a line, which separates the area of pure liquid from that of the two-phase mixture, Liquid+Gas. Meanwhile, the composition, where the boiling point is equal to T_1, forms another line which distinguishes the pure gas area from the two-phase mixture.

2.1.1 The boiling point of a metal-hydrogen solution

From the definition of the boiling point, we have

$$P_{ext} = P_{vap} + P_{H_2} \quad \ldots\ldots\ldots\ldots\ldots\ldots (1)$$

where $\mathbf{P_{ext}}$ is the external pressure;

$\mathbf{P_{vap}}$ is the vapor pressure of the metal;

$\mathbf{P_{H2}}$ is the partial pressure of hydrogen.

To be illustrated on the phase diagram, the equation (1) should be transformed into a form expressed by the temperature T and the composition of hydrogen X_H. We have

$$X_H = \frac{[H]}{[metal] + [H]} = \frac{2[H_2]}{[metal] + 2[H_2]} = \frac{2P_{H_2}}{P_{vap} + 2P_{H_2}} \quad \ldots\ldots\ldots (2)$$

where the [ ] represents the mole fraction.

Substitute (1) in (2):

$$X_H = \frac{2(P_{ext} - P_{vap})}{2P_{ext} - P_{vap}} \quad \ldots\ldots\ldots\ldots\ldots\ldots\ldots (3)$$

In (3), Pvap is a function of temperature, which obeys:

$$\mathrm{Log}\,(P_{vap}) = -\frac{A}{T} + B + C \times \mathrm{Log}\,(T) + 0.001 \times D \times T \ldots\ldots (4)$$

Combining (3) and (4), if Pext is known, hence we have the line of the boiling points.

The constants are from the reference.[3] When Pvap is in torr and T is in Kelvin, the constants for Cu and Mg are as following:

Metal	Temp. range(K)	A	B	C	D
Cu	298~1356	17870	10.63	-0.236	-0.16
	1356~2870	17650	13.39	-1.273	---
Mg	298~922	7780	11.41	-0.855	---
	922~1363	7550	12.79	-1.41	---

2.1.2 Solubility of H in a liquid metal

When hydrogen dissolves in a metal, it is in its atomic form rather than molecular. The reaction thus can be described as:

$$H_2 = 2\underline{H} \ldots\ldots (5)$$

where the equilibrium constant K' is expressed as:

$$K' = \frac{X_H^{\,2}}{P_{H_2}} \ldots\ldots (6)$$

Then the Sieverts law is obtained:

$$X_H = K\left(P_{H_2}\right)^{1/2} \ldots\ldots (7)$$

Where $K=(K')^{1/2}$.

The Sieverts law constant K is usually characterized by its temperature dependence and hence given in literature in the form:

$$\mathrm{Log}(K) = \frac{A'}{T} + B' \quad \ldots\ldots (8)$$

Combining (7) and (8) results in:

$$\mathrm{Log}(X_H) = \frac{A'}{T} + B' + \frac{1}{2}\mathrm{Log}\left(P_{H_2}\right) \quad \ldots\ldots (9)$$

where X_H is mole/mole, T is in Kelvin, P_{H2} is in atm.

Substitute (1) into (9), we have:

$$\mathrm{Log}(X_H) = \frac{A'}{T} + B' + \frac{1}{2}\mathrm{Log}(P_{ext} - P_{vap}) \quad \ldots\ldots (10)$$

where Pvap is a function of T, obeying equation (4).

The solubilities of H in metals are measured at temperatures close to their melting points, where Pvap is very small comparing with Pext. Therefore, $P_{H_2} \approx P_{ext}$, and

$$\mathrm{Log}(X_H) \approx \frac{A'}{T} + B' + \frac{1}{2}\mathrm{Log}(P_{ext}) \quad \ldots\ldots (11)$$

Using the data from the reference[4], plots of $\mathrm{Log}(X_H)$ vs. 1/T for different metals(Figure 2.2-Figure 2.8) can be obtained. For each metal, there is one set of constants(A' and B') for any of its possible condensed phases, which usually are the liquid phase and the solid phase. When X_H is in the unit of mole/mole, T is in Kelvin and Pext is in atm, the constants for some typical metals are listed in the following table:[4]

Metal	phase	A'	B'
Ag	Liquid	-1.30	-3512
	Solid	-1.66	-3600
Al	Liquid	-1.08	-3086
	Solid	-1.95	-3300
Co	Liquid	-1.21	-2140
	Solid	-1.83	-1680
Cu	Liquid	-1.84	-1737
	Solid	-2.29	-1867
Fe	Liquid	-1.43	-1660
	α–Fe	-2.25	-1268
	γ–Fe	-1.83	-1562
	δ–Fe	-1.86	-1504
Mg	Liquid	-2.24	-716
	Solid	-0.93	-776
Ni	Liquid	-1.42	-1176
	Solid	-2.00	-870

2.2 SOLID VS. LIQUID

Two characteristic lines make up the borders of three areas: the solid phase, the two-phase mixture of solid and liquid, and the liquid phase(Figure 2.1). Named after the neighboring primary phase, one is the solidus line, and the other is the liquidus line.

2.2.1 the liquidus line

Under the condition of equilibrium, the chemical potential of the metal in liquid is the same as

that in solid. So we have:

$$\mu_A^L = \mu_A^\alpha \quad \ldots\ldots (11)$$

where $\mu^L{}_A$ represents the chemical potential of the metal in the liquid phase, and $\mu^\alpha{}_A$ is that of the metal in the solid phase.

From equation (11), we have:

$$\mu_A^{o,L} + RT \times \ln a_A^L = \mu_A^{o,\alpha} + RT \times \ln a_A^\alpha \quad \ldots\ldots (12)$$

where $\mu_A^{o,L}$ and $\mu_A^{o,\alpha}$ are respectively the chemical potentials of the liquid metal and the solid metal in their standard states;

a_A^L and a_A^α are respectively the activity functions of the metal in the liquid phase and in the solid phase.,

Further, $RT \times \ln \frac{a_A^L}{a_A^\alpha} = -\left(\mu_A^{o,L} - \mu_A^{o,\alpha}\right) = -\Delta\mu_A^{o,\alpha \to L}$, or

$$\ln \frac{a_A^L}{a_A^\alpha} = -\frac{\Delta H_{f,A}^o}{R}\left(\frac{1}{T} - \frac{1}{T_{f,A}}\right) \quad \ldots\ldots (13)$$

Usually, a solid metal has a very low solubility of hydrogen, thus can be approximately regarded

as pure, which implies $a_A^{\alpha} \approx 1$, therefore,

$$\ln a_A^L = -\frac{C1}{T} + C2 \quad \ldots\ldots (14)$$

Because the liquid-hydrogen binary solution is very dilute, it can be treated as an ideal solution. Thus,

$$\ln a_A^L \approx \ln X_A^L = \ln\left(1 - X_H^L\right) \quad \ldots\ldots (15)$$

For the metal-hydrogen solution, we have $X_H^L \ll 1$, thus

$$X_H^L \approx -\ln\left(1 - X_H^L\right) \approx -\ln a_A^L = \frac{C1}{T} - C2 \quad \ldots\ldots (16)$$

which is the expression of the liquidus line.

Also from equation(13) and (14),

$$\ln a_A^{\alpha} = \frac{C3}{T} - C4$$

and further, we have $X_H^{\alpha} = \frac{C3}{T} - C4 \quad \ldots\ldots (17)$

which is the expression of the solidus line. C1, C2, C3, C4 are constants to be determined, and vary with different metals.

When X_H is in mole/mole and T is in Kelvin, the constants for Cu and Mg are listed in the following table:[5,6]

Metal	C1	C2	C3	C4
Cu	1375	1.014	458	0.338
Mg	2044	2.214	1363	1.476

2.3 SOLID VS. GAS

Two lines separate the three regions: the solid phase, the two-phase mixture of solid and gas, and the gas phase(Figure 2.1). The line between the solid and the solid+gas is the line of solubilities of hydrogen in the solid metal at different temperatures. Consequently it has exactly the same expression as equation (10) with the only difference in the constants. Similarly, the line between solid+gas and gas has the form of equation (3) with the only difference in the constants for the P_{vap}.

2.4 EUTECTIC POINT

The eutectic point, the cross-end of the liquidus line and the solubility line in Figure 2.1, is the lowest temperature that the liquid phase can exist, where the eutectic reaction happens:

$$\text{Liquid} \rightarrow \text{Solid} + \text{Gas}$$

2.5 PHASE DIAGRAM OF Cu-H AND Mg-H SYSTEMS

The phase diagrams of Cu-H and Mg-H are obtained by combining all those lines calculated with appropriate constants. Since the solubility of H is proportional to the square root of the external hydrogen pressure, a desired level of porosity in the material can be reached by carefully controlling the hydrogen pressure. The phase diagrams for a normal pressure(~1 atm) and a high pressure(~100 atm) are calculated and presented on Figure2.9-Figure2.13. The change of the melting

point due to the raising of the pressure is proved by the Clausius-Claperon equation to be very small and negligible.

3. EFFECT OF A THIRD COMPONENT ON THE EUTECTIC POINT

3.1 THE EFFECT OF A THIRD COMPONENT TO A SOLID-GAS ALLOY

In the real world, there are always some small amounts of other components involved in a metal-hydrogen solution. Therefore, the effect of additions of a third component on the temperature and composition of the eutectic point is important for the solidification process. An analytical solution is derived and presented in the following work, which is based on Lupis' theory.[7]

Consider the binary eutectic system 1-2 in Figure 3.1 and the effect of a small addition of a component 3 at the temperature T_E+dT. Lupis has given the analytic derivation of the effect of the component 3 on the eutectic temperature T_E and the eutectic composition X_{2E}:

$$\left(\frac{dT}{dX_3}\right)_E = E_{12}\left(1-\frac{X_2^E-X_2^\alpha}{X_2^\beta-X_2^\alpha}\left(\frac{\gamma_3^{\infty(l,E)}}{\gamma_3^{\infty(\beta,B)}}\exp\frac{\mu^{*(l)}_3-\mu^{*(\beta)}_3}{RT_E}\right)-\frac{X_2^\beta-X_2^E}{X_2^\beta-X_2^\alpha}\left(\frac{\gamma_3^{\infty(l,E)}}{\gamma_3^{\infty(\alpha,A)}}\exp\frac{\mu^{*(l)}_3-\mu^{*(\alpha)}_3}{RT_E}\right)\right) \quad \ldots\ldots (1)$$

and

$$\left(\frac{dX_2}{dX_3}\right)_E = \left(\frac{dX_2^{l(\alpha)}}{dX_3^{l(\alpha)}}\frac{dX_2^{l(\beta)}}{dT}-\frac{dX_2^{l(\beta)}}{dX_3^{l(\beta)}}\frac{dX_2^{l(\alpha)}}{dT}\right)\Big/\left(\frac{dX_2^{l(\beta)}}{dT}-\frac{dX_2^{l(\alpha)}}{dT}\right) \ldots (2)$$

where

$$E_{12} = \left(\frac{dT}{dX_3}\right)_{E,\,lim} = \frac{-1}{\left|\frac{RQ}{dT}\right|}\frac{X_1^E X_2^E}{\psi^l}\frac{\left(X_2^\beta - X_2^\alpha\right)}{\left(X_2^\beta - X_2^E\right)\left(X_2^E - X_2^\alpha\right)} \quad \ldots\ldots (3)$$

In these equations, $\gamma_3^{\infty(l,E)}$, $\gamma_3^{\infty(\alpha,A)}$ are respectively the activity coefficients of 3 at infinite dilution in the liquid phase of eutectic composition E and in the α phase of composition A(see Figure 3.1). $\mu^*{}_3^{(l)}$, $\mu^*{}_3^{(\alpha)}$ are the reference values of the chemical potentials of component 3 in the liquid phase and in the α phase. ψ^l is the stability function of the metal-hydrogen binary system, in the liquid phase.

At equilibrium of α and liquid, where $T=T_E$, the chemical potential of the third component in each phase is the same. Thus, $\mu_3^{(\alpha)} = \mu_3^{(l)}$, which leads to[8]

$$\ln\frac{X_3^\alpha}{X_3^l} + \ln\gamma_3^\alpha - \ln\gamma_3^l - \frac{1}{RT_E}\Delta\mu_3^{\circ(\alpha\to l)} = 0 \quad \ldots\ldots (4)$$

where X_3^α, X_3^l are the mole fractions of component 3 in the α phase and in the liquid phase,

γ_3^α, γ_3^l are respectively the activity coefficient of component 3 in the α phase and in the liquid phase,

$\Delta\mu_3^{\circ(\alpha\to l)}$ is the difference in the values of the chemical potential of 3 in the two structures α and liquid, when it is in its standard state.

$$\Rightarrow \qquad \gamma_3^\alpha = \gamma_3^l\frac{X_3^l}{X_3^\alpha}\exp\left[\frac{\Delta H_{f,3}^\circ}{R}\left(\frac{1}{T_E} - \frac{1}{T_{m,3}}\right)\right] \quad \ldots\ldots (5)$$

where $\Delta H^{\circ}_{f,3}$ is the heat of fusion of component 3 in its standard state,

$T_{m,3}$ is the melting point of pure component 3.

$$\text{Since } X_3 \text{ is very small, } \Rightarrow \gamma_3^{\infty,\alpha} = \gamma_3^{\infty,1}\frac{X_3^1}{X_3^{\alpha}}\exp\left[\frac{\Delta H^{\circ}_{f,3}}{R}\left(\frac{1}{T_E}-\frac{1}{T_{m,3}}\right)\right] \quad \ldots (6)$$

For the same reason,

$$\gamma_3^{\infty,\beta} = \gamma_3^{\infty,1}\frac{X_3^1}{X_3^{\beta}}\exp\left[\left(-\frac{\Delta H^{\circ}_{evap,3}}{R}\right)\left(\frac{1}{T_E}-\frac{1}{T_{b,3}}\right)\right] \quad \ldots\ldots\ldots (7)$$

where $\Delta H^{\circ}_{evap,3}$ is the heat of vaporization of component 3 in its standard state,

$T_{b,3}$ is the boiling point of pure component 3.

Also we have

$$\exp\frac{\mu^{*(1)}_3 - \mu^{*(\beta)}_3}{RT_E} = \exp\left[\left(-\frac{\Delta H^{\circ}_{evap,3}}{R}\right)\left(\frac{1}{T_E}-\frac{1}{T_{b,3}}\right)\right] \quad \ldots\ldots (8)$$

and

$$\exp\frac{\mu^{*(1)}_3 - \mu^{*(\alpha)}_3}{RT_E} = \exp\left[\frac{\Delta H^{\circ}_{f,3}}{R}\left(\frac{1}{T_E}-\frac{1}{T_{m,3}}\right)\right] \quad \ldots\ldots\ldots (9)$$

Substitute equation(6)-(9) into (1):

$$\left(\frac{dT}{dX_3}\right)_E = E_{12}\left(1-\frac{X_2^E - X_2^{\alpha}}{X_2^{\beta} - X_2^{\alpha}}\cdot\frac{X_3^{\beta}}{X_3^1} - \frac{X_2^{\beta} - X_2^E}{X_2^{\beta} - X_2^{\alpha}}\cdot\frac{X_3^{\alpha}}{X_3^1}\right) \quad \ldots\ldots\ldots\ldots (10)$$

Since the vapor pressure of the component 3 in the solid phase is extremely low, the second term

on the right side of the equation can be ignored. Thus,

$$\left(\frac{dT}{dX_3}\right)_E = E_{12}\left(1-\frac{X_2^{\beta}-X_2^{E}}{X_2^{\beta}-X_2^{\alpha}}\cdot\frac{X_3^{\alpha}}{X_3^{1}}\right) \quad \text{.....(11)}$$

For metal-hydrogen alloys, $X_2^{\beta} \approx 1 \gg X_2^{E}, X_2^{\alpha}$, so $\dfrac{X_2^{\beta}-X_2^{E}}{X_2^{\beta}-X_2^{\alpha}} \approx 1$, and equation(11) can be

further simplified as:

$$\left(\frac{dT}{dX_3}\right)_E = E_{12}\left(1-\frac{X_3^{\alpha}}{X_3^{1}}\right) \quad \text{.....(12)}$$

Substitute equation(6)-(9) into (2):

,

$$\left(\frac{dX_2}{dX_3}\right)_E = \frac{X_2^{E}}{\left|\frac{RQ}{dT}\right|\psi^{1}}\left(\left\{\frac{X_1^{E}}{X_2^{E}-X_2^{\alpha}}\cdot\frac{X_3^{\alpha}}{X_3^{1}}-\frac{X_1^{\alpha}}{X_2^{E}-X_2^{\alpha}}-\frac{\partial}{\partial X_3^{1}}\ln\gamma_2^{1}\right\}\cdot\frac{dX_2^{1(\beta)}}{dT}\right.$$

$$\left.-\left\{\frac{X_1^{E}}{X_2^{E}-X_2^{\beta}}\cdot\frac{X_3^{\beta}}{X_3^{1}}-\frac{X_1^{\beta}}{X_2^{E}-X_2^{\beta}}-\frac{\partial}{\partial X_3^{1}}\ln\gamma_2^{1}\right\}\cdot\frac{dX_2^{1(\alpha)}}{dT}\right) \quad \text{.....(13)}$$

3.2 THE EFFECT OF A THIRD COMPONENT TO Cu-H SYSTEM

From the phase diagram of Cu-H system,

$$\left|\frac{RQ}{dT}\right| \approx 0.00075\ (K^{-1} \cdot \text{atom/atom}), \qquad \Psi^{l} \approx 1,$$

$$X_1^E = 0.997\ (\text{atom/atom}), \quad X_2^E = 0.003\ (\text{atom/atom}),$$

$$X_2^{\beta} \cong 1\ (\text{atom/atom}), \qquad X_2^{\alpha} = 0.001\ (\text{atom/atom})$$

Substitute these data in equation(3), then the maximum change of temperature is:

$$\left.\frac{dT}{dX_3}\right|_{E,\,lim} = E_{12} = -19.98\ \text{K/atom\%} \qquad (14)$$

Thus, for Cu-H,

$$\left.\frac{dT}{dX_3}\right|_{E} = -19.98\left(1 - \frac{X_3^{\alpha}}{X_3^{l}}\right)\ \text{K/atom\%} \qquad (15)$$

Substitute the data in equation(13),

$$\left.\frac{dX_2}{dX_3}\right|_{E} = -0.0154\left(1 - \frac{X_3^{\alpha}}{X_3^{l}}\right) - 0.003\left(\frac{\partial}{\partial X_3^{l}} \ln \gamma_2^{l}\right) \qquad (16)$$

The value of $\frac{X_3^{\alpha}}{X_3^{l}}$ can be estimated from the phase diagram of the third component vs. copper. The

term $\frac{\partial}{\partial X_3^l}\ln\gamma_2^l$ is actually an interaction coefficient of the component 3 in binary liquid copper alloys. The value of it for some elements is listed in the following table[9]:

Element	$\frac{\partial}{\partial X_3^l}\ln\gamma_2^l$
Ag	-2.5
Al	14.0
Au	3.7
Bi	-6800/T+1.65
Ca	20.0
Fe	-5.7
Ga	7.0
Ge	13.4
Mg	9.8
Mn	6.0
O	-24,000/T+7.8
Pb	-2.7
S	-20800/T
Sb	15.0
Sn	10.0
Tl	-4.8
Zn	4.0

If Ag, Al or Mg is added into the liquid copper, $X_3^\alpha < X_3^l$, thus $\left.\frac{dT}{dX_3}\right|_E < 0$, which means the eutectic temperature decreases due to the third component.

If Co, Fe, or Ni is added into the liquid copper, $X_3^{\alpha} < X_3^{l}$, therefore, $\left.\frac{dT}{dX_3}\right|_E > 0$, which means the eutectic temperature is raised by the effect of the third component.

The composition of the eutectic point may either increase or decrease, depending on the value of $\frac{X_3^{\alpha}}{X_3^{l}}$ and $\frac{\partial}{\partial X_3^{l}} \ln \gamma_2^{l}$.

4. SOLIDIFICATION KINETICS OF THE METAL-HYDROGEN ALLOYS

The solidification process of the metal-hydrogen alloys starts from a nucleation process, and is completed by the growth of the nuclei into the surrounding liquid. The bubble nucleation process has been well studied by Sridhar[5]. The following work will be concentrated on the growth process. In many cases, a rod-like metal-hydrogen eutectic is wanted. With the assumption of a steady-state growth, the Jackson-Hunt theory[10] is applied here, which is able to predict the relations among the scale of each phase, the growth rate of the eutectics and the average undercooling around the front of growth. Furthermore, by comparing the growth rate of the eutectics with that of the primary phase, we can figure out what type of growth(coupled eutectic growth or primary dendrites growth) is preferred under varying conditions(temperature, pressure and temperature gradient).

4.1 GROWTH OF EUTECTICS

Ignoring the initial nucleation, if the external pressure is fixed, we can regard the growth of eutectics as a steady state process. The experimental works show that rod eutectic growth usually happens, or the hydrogen gas forms cylinders embedded in the solid metal. Because there is no faceting behavior during the growth, it can be regarded as a growth in normal eutectic solidification. According to the Jackson-Hunt theory, by labelling the gas phase as α and the solid phase as

β, we have the relation:

$$\frac{\Delta T}{m} = \upsilon R Q^R + \frac{a^R}{R} \quad \ldots\ldots (1)$$

where ΔT is the average undercooling at the interface;

υ is the growth rate of the interface;

R is defined as: $R = r_\alpha + r_\beta = r_\alpha\sqrt{1+\zeta}$,

r_α, r_β are respectively the radius of the gas phase and the solid phase, and are illustrated in Figure 4.1,

ζ is the volume ratio of the two phases, and $\zeta = \dfrac{\left(r_\alpha + r_\beta\right)^2 - r_\alpha^2}{r_\alpha^2}$;

$m = \dfrac{1}{\dfrac{1}{m_\alpha} + \dfrac{1}{m_\beta}}$, m_α and m_β are the slopes of the α and β liquidus lines;

$$Q^R = \frac{4(1+\zeta)}{D\zeta} C_0 M \quad \ldots\ldots (2),$$

where D is the diffusion coefficient of H in the metal.

$C_0 = C_\alpha - C_\beta$, C_α, C_β are respectively the mole fractions of hydrogen in the gas phase and the solid phase.

$$M = \sum_{n=1}^{\infty} \frac{1}{\gamma_n^3} \frac{J_1^2\left(\dfrac{r_\alpha \gamma_n}{r_\alpha + r_\beta}\right)}{J_0^2(\gamma_n)}$$

$J_0(x)$ and $J_1(x)$ are respectively the Bessell functions with the order of 0 and the order of 1. γ_n is the root of $J_1(x)=0$.

$$a^R = 2\sqrt{1+\zeta}\left(\frac{a_\alpha^R}{m_\alpha} + \frac{a_\beta^R}{\zeta m_\beta}\right) \quad \ldots\ldots\ldots\ldots\ldots\ldots\ldots (3),$$

a_α^R and a_β^R are constants given by the Gibbs-Thompson relationship,

$$a_\alpha^R = \frac{\sigma_\alpha^R R T_E^2}{P_{ext}\Delta H^o}\sin\theta_\alpha^R, \text{ and } a_\beta^R = (T_E/L)_\beta \sigma_\beta^R \sin\theta_\beta^R,$$

ΔH^o is the heat of reaction that hydrogen dissolves into the liquid metal.

T_E is the eutectic temperature.

σ_α^R and σ_β^R are the specific surface free energies of the α-liquid and β–liquid interfaces, respectively.

θ_α^R and θ_β^R are the contact angles described in Figure 4.2. At the growing boundary between Gas and Metal.

$\sigma_{Solid-Gas} \approx \sigma_{Solid-Liquid} + \sigma_{Gas-Liquid}$. Thus, $\theta_\alpha^R, \theta_\beta^R \approx 90°$, and $\sin\theta_\alpha^R, \sin\theta_\beta^R \approx 1$.

There are three variables, ΔT, υ and R in equation(1). Thus an additional condition must be specified to solve equation(1) for R in terms of one other variable. The simplest condition is that proposed by Zener[11] and adopted by Tiller[12] and Hillert[13], in which is was assumed that the solid grows at the extremum, or at the minimum undercooling or the maximum growth rate. For equation(1), the ΔT has a minimum when

$$R^2\upsilon = a^R/Q^R \quad \ldots\ldots\ldots\ldots\ldots\ldots\ldots (4)$$

$$\text{or} \qquad \Delta T^2/\upsilon = 4m^2 a^R Q^R \quad \ldots\ldots (5)$$

$$\text{or} \qquad \Delta T \times R = 2ma^R \quad \ldots\ldots (6)$$

4.1.2 Eutectic Growth in the Cu-H system

With the help of the phase diagrams and some references, the eutectic growth of the Cu-H at the eutectic positions can be estimated as following. For the Cu-H system, if the external pressure is 100 atm, according to the phase diagram(Figure2.11),

$$C_{Liq}\big|_{@\text{Eutectic point}} = 0.003, \quad C_\beta = 0.001, \; C_\alpha = \frac{2P_{ext}}{RT_E},$$

where α represents for the gas phase, β is for the solid phase.

The volume ratio $\zeta = \dfrac{\left(r_\alpha + r_\beta\right)^2 - r_\alpha^2}{r_\alpha^2}$.

From the mass conservation during the growth,

$$C_\alpha r_\alpha^2 + C_\beta\left((r_\alpha + r_\beta)^2 - r_\alpha^2 \right) = C_{Liq}\left((r_\alpha + r_\beta)^2 - r_\alpha^2 \right)$$

therefore, combining the above two equations, we have, $\zeta = \dfrac{C_\alpha}{C_{Liq} - C_\beta}$.

Put in the data of $P_{ext} = 100$ atm, and $T_E = 1352$ K, then the volume ratio is obtained:

$\zeta = 6.37$.

Further, $M(\zeta = 6.37) = 0.04$, and $Q^R = 1.85 \times 10^6 \quad s \cdot m^{-2}$.

Also, for Copper-Hydrogen,[14,15]

$$\sigma_{solid}^{Liq} = 0.177 \ J \cdot m^{-2}, \quad \sigma_{gas}^{Liq} = 1.31 \ J \cdot m^{-2}, \ \sigma_{gas}^{solid} = 1.6 \ J \cdot m^{-2}.$$

and[5]

$$\Delta H° \approx 7.78 \times 10^4 \ J/mol, \ m_\alpha = 1.3 \times 10^5 \ K, \ m_\beta = 1233.3 \ K.$$

Substitute all these data into equation (3), and we have, $a^R = 1.08 \times 10^{-9}$ m. And finally we have the characteristic constant for the eutectic growth of the Cu-H system under the extremum condition:

$$R^2 \upsilon = \frac{a^R}{Q^R} \approx 5.84 \times 10^{-10} \ cm^3/s \ .$$

For a comparison, a normal eutectic system like Pb-Sn, has the constant[16]:

$$\lambda^2 \upsilon = 3.30 \times 10^{-11} \ cm^3/s$$

So the solid-gas eutectics is similar to the conventional eutectics in the relations between the scale of the coupled phases and the growth rate.

4.2 DENDRITE GROWTH IN EUTECTIC ALLOYS

Good microstructural control of the alloys is essential in obtaining the required properties. Primary phases present in a eutectic matrix may have either a beneficial or a detrimental effect on these properties. Therefore, their appearance must be carefully controlled. The growth of such dendrite structure in eutectics has been studied by Kurz and Fisher[17]. The overall form of the

growth in terms of the undercooling and the growth rate is given by:

$$\Delta T_{dend} = GD/\upsilon_{dend} + K\sqrt{\upsilon_{dend}} \quad \ldots\ldots (5)$$

where, υ_{dend} is the growth rate, G is the temperature gradient at the interface and,

$$K = A\,[-mC(1-k)\theta/D]^{0.5} \quad \ldots\ldots (6)$$

In this equation, A=2.83; C is the initial alloy composition; m is the liquidus slope; k is the distribution coefficient; θ is the Gibbs-Thompson coefficient; D is the diffusivity of hydrogen in the liquid metal.

4.3 THE COUPLED ZONE

The coupled zone is defined as the range of conditions (generally composition and undercooling values) at which the two eutectic phases can grow with similar velocities. Many factors have influence over the stability of eutectic structure. Among them, the growth of a single phase in dendrites is the most important. To estimate its effect, the simple competitive growth approach is applied, which points out that the morphology appearing in the microstructure, under given conditions, will be those having the lowest interface undercooling or the highest growth rate[17]. Therefore, the eutectic-stable zone is the certain range in which the eutectic could grow faster than primary crystals.

Figure 4.3 shows that when the temperature in the range between T_E and T^*, for the same growth rate, the eutectic growth needs lower undercooling, therefore, according to the extremum condition, the eutectic growth is preferred to the primary dendrite growth. Figure 4.4 is the illustration of the eutectic stable range (T_E-T_*) with varying concentration on the phase diagram, which is called the couple zone. The right side of the coupled zone is limited by the solubility of hydrogen in the liquid metal. Exceeding this limit will lead to the appearance of pores in the liquid, therefore, should be avoided during the solidification process.

A program has been written to compare the eutectic growth with the dendrite growth, and gives the coupled zone on the phase diagram. Figure 4.5-4.6 are the results of the program for Cu-H and Mg-H systems.

5. SUMMARY

The phase diagrams of different metal-hydrogen systems are similar. The eutectic point is usually about several degrees below the melting point of the pure metal, and is determined by the external hydrogen pressure. A third component will change both the temperature and the composition of the eutectic point. The uncertainty of the eutectic point is one reason that causes the solidification process hard to control.

The eutectic growth of the coupled solid-gas phases is similar to some conventional solid-solid eutectic systems in the scale of phases and the growth rate. Because of the very unbalance of the phase diagram, the eutectic stable region, or the coupled zone, is very skewed. The stable range for any composition is always less than several degrees, which is probably the biggest reason for the extraordinary difficulty in controlling the gas-eutectic solidification. The temperature gradient may play an important role during the process. Since a high temperature gradient slows down the growth of the primary dendrites, therefore, the eutectic stable range is expanded. So practically, to cool down the metal-hydrogen solution more rapidly during the solidification process is much more likely to have solid-gas eutectics formed.

REFERENCES

1. D.M. Walukas; GASAR Materials: A Novel Approach in the Fabrication of Porous Materials, DMK TEK INC., 1992;
2. Sandia researchers study Porous CIS Aerospace Metals&News&Update, JOM, Vol.46, No.9, 1994, p.8;
3. Colin J. Smithells; Metals Reference Book, Fifth Edition, Butterworth & Co(Publishers) Ltd 1976, p.231;
4. E. Fromm & E. Gebhardt; Gase und Kohlenstoff in Metallen, Springer-Verlag Berlin Heidelberg New York 1976;
5. S. Sridhar; Master Thesis;
6. V.I. Shapovalov, A.P. Semik, and A.G. Timchenko; On the Solubility of Hydrogen in Liquid Magnesium, Izvestiya Rossiiskoi Akademii Nauk. Metally, No.3, pp. 25-28, 1993
7. C.H.P. Lupis; Effect of Small Additions of a Third Component on the Eutectic and Peritectic Temperatures of Binary Systems, Metallurgical Transactions B, Vol. 9B, June 1978, p.231;
8. C.H.P. Lupis; Chemical Thermodynamics of Materials, c1983, New York: North-Holland, p.219.
9. G.K. Sigworth and J.F. Elliott; The thermodynamics of dilute liquid copper alloys, Canadian Metallurgical Quaterly, Vol. 13, No. 3, 1973, p.455-461;
10. K.A. Jackson and J.D. Hunt; Lamellar and Rod Eutectic Growth, Transactions of the Metallurgical Society of AIME, Vol. 236, August 1966, p.1129-1142;
11. C. Zener; AIME Trans., 1946, Vol. 167, pp. 550;
12. W. A. Tiller; Liquid Metals and Solidification, p.276-318, ASM, Cleveland. 1958;
13. M. Hillert: Jernkontorets Ann., 1960, Vol. 144, p.520;
14. Andries Rinse Miedema and Robertus Boom; Surface Tension and Electron Density of Pure Liquid Metals, Z. Metallkde., Bd69(1978)H.3, p.183-190;
15. Andries Rinse Miedema; Surface Energies of Solid Metals, Z. Metallkde. Bd.69(1978)H.5, p.287-292;
16. J.D. Hunt and J.P. Chilton; J. Inst. Metals, 1963, Vol. 92, p.21;
17. W. Kurz and D.J. Fisher; Dendrite growth in eutectic alloys: the coupled zone, International Metals Reviews, 1979 Nos.5 and 6, p.177-204;

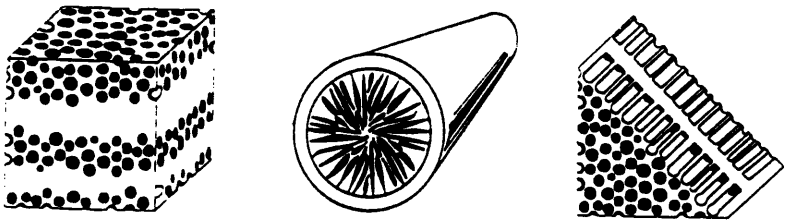

Figure 1.1 GASAR materials with different porous structures

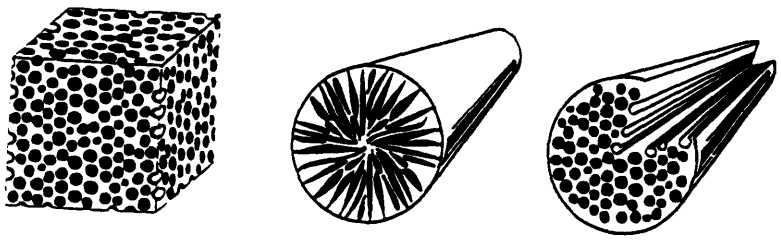

Figure 1.2 GASAR materials with different porous densities and distributions

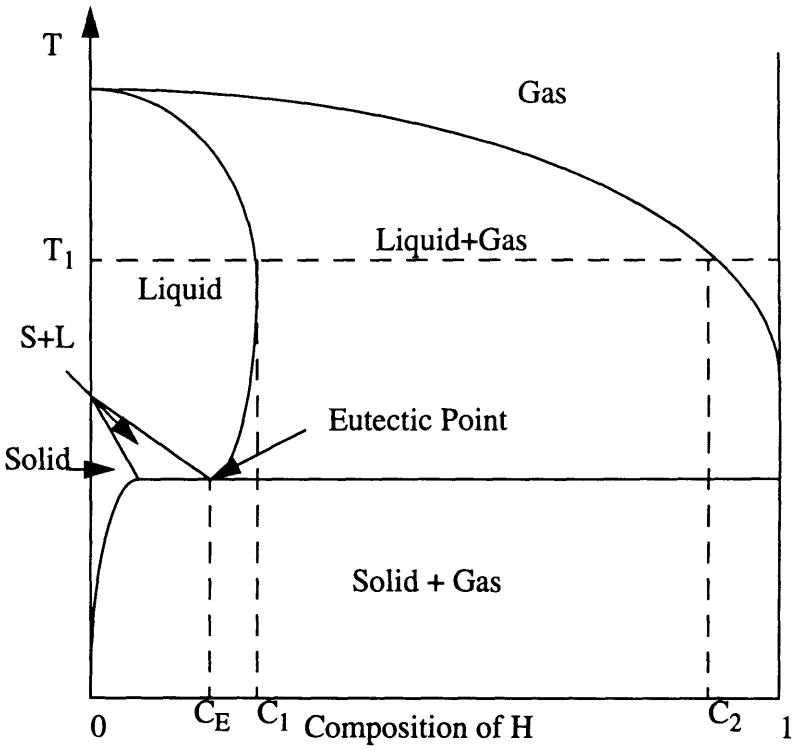

Figure 2.1 Schematic phase diagram of a metal-hydrogen system

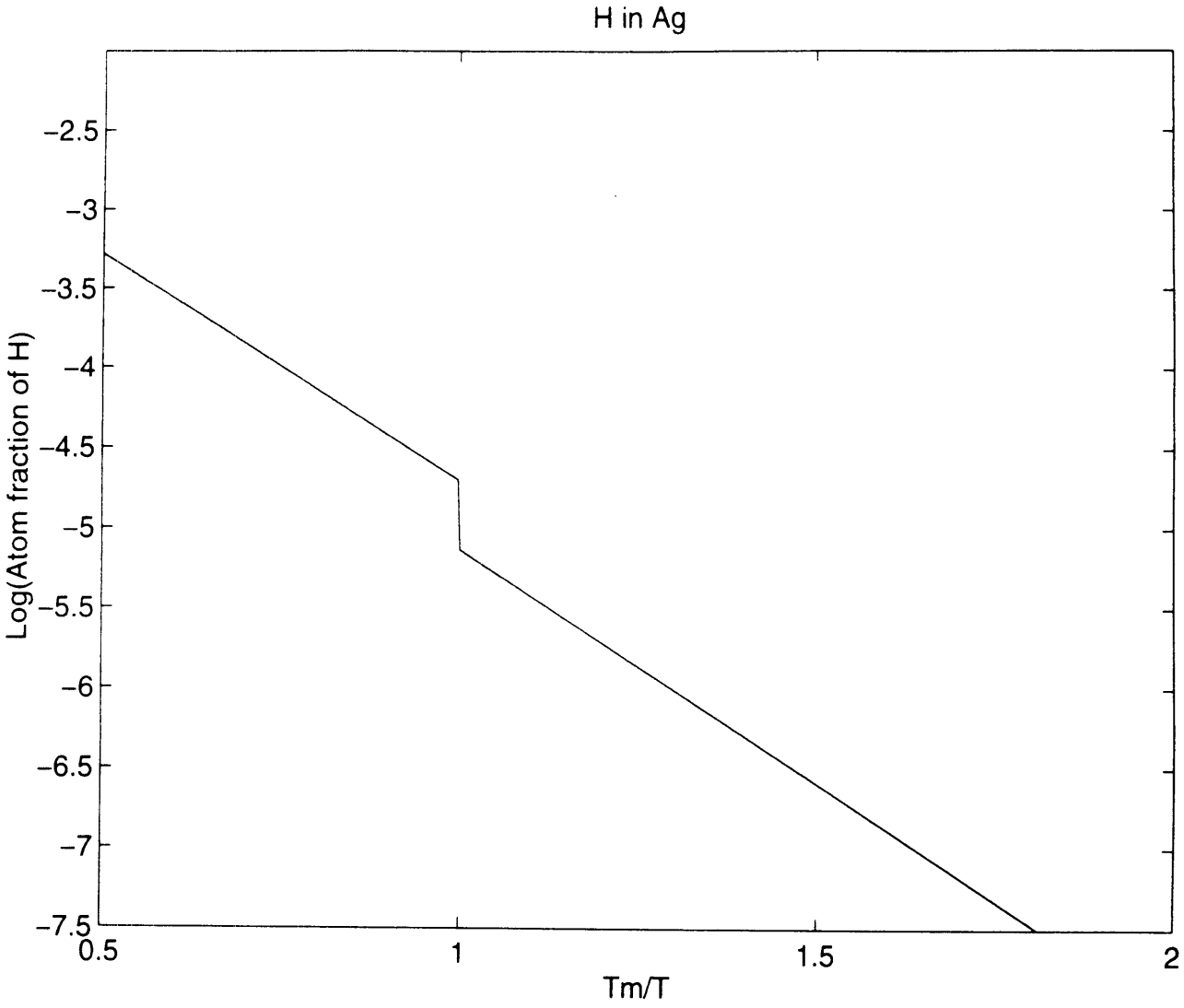

Figure 2.2 Solubility of hydrogen in Ag (P_{H2} = 1 atm)

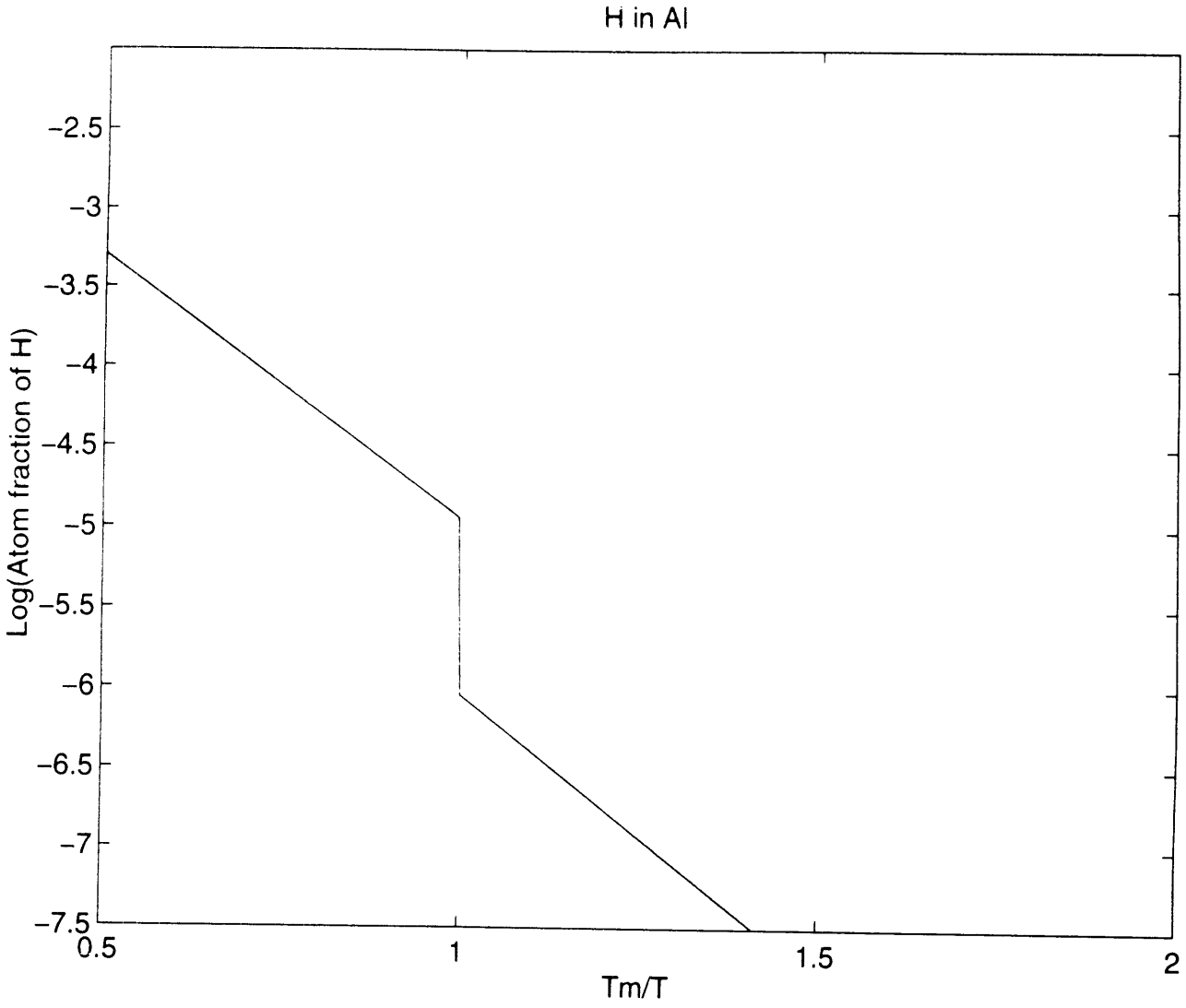

Figure 2.3 Solubility of hydrogen in Al (P_{H2} = 1 atm)

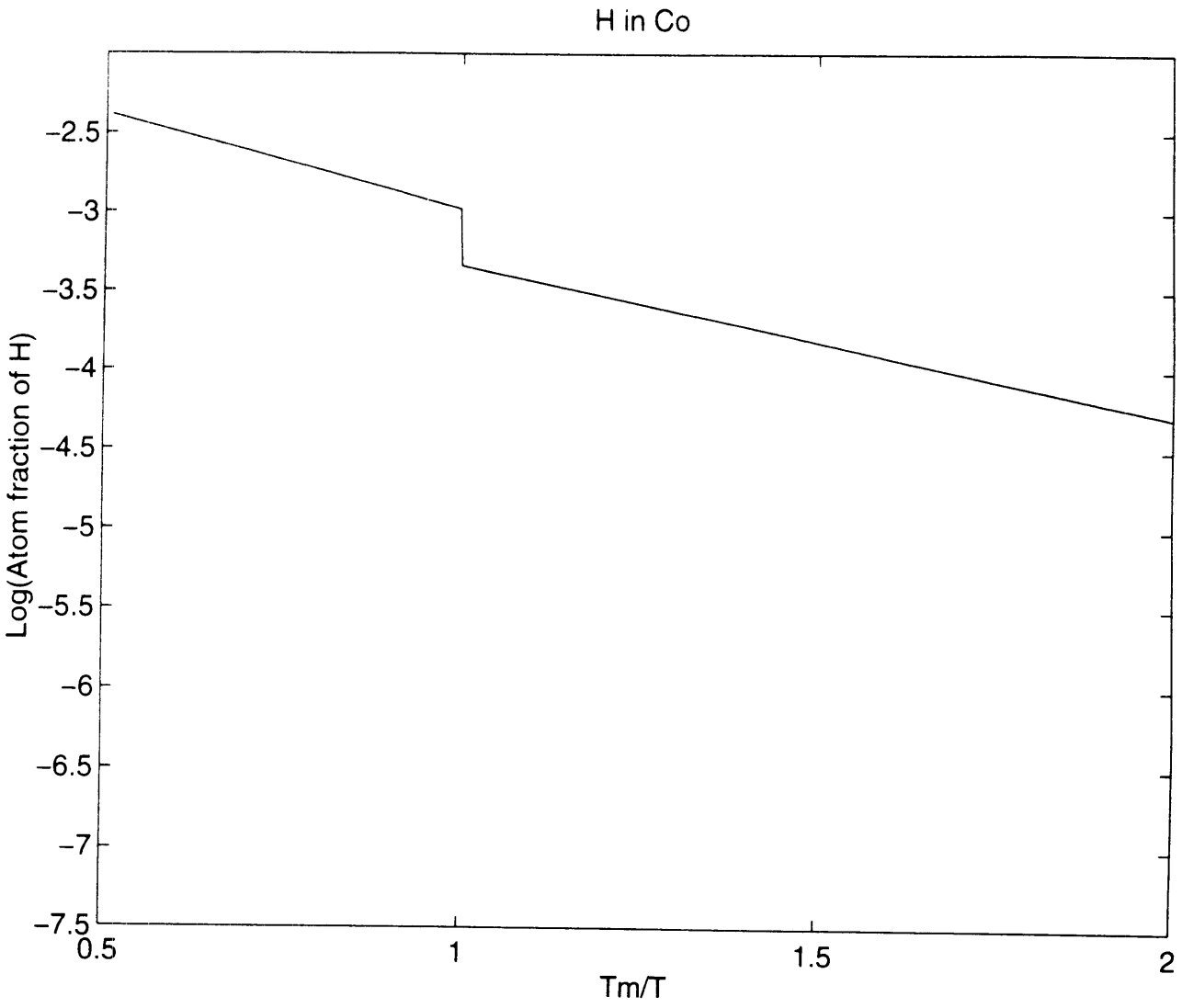

Figure 2.4 Solubility of hydrogen in Co (P_{H2} = 1 atm)

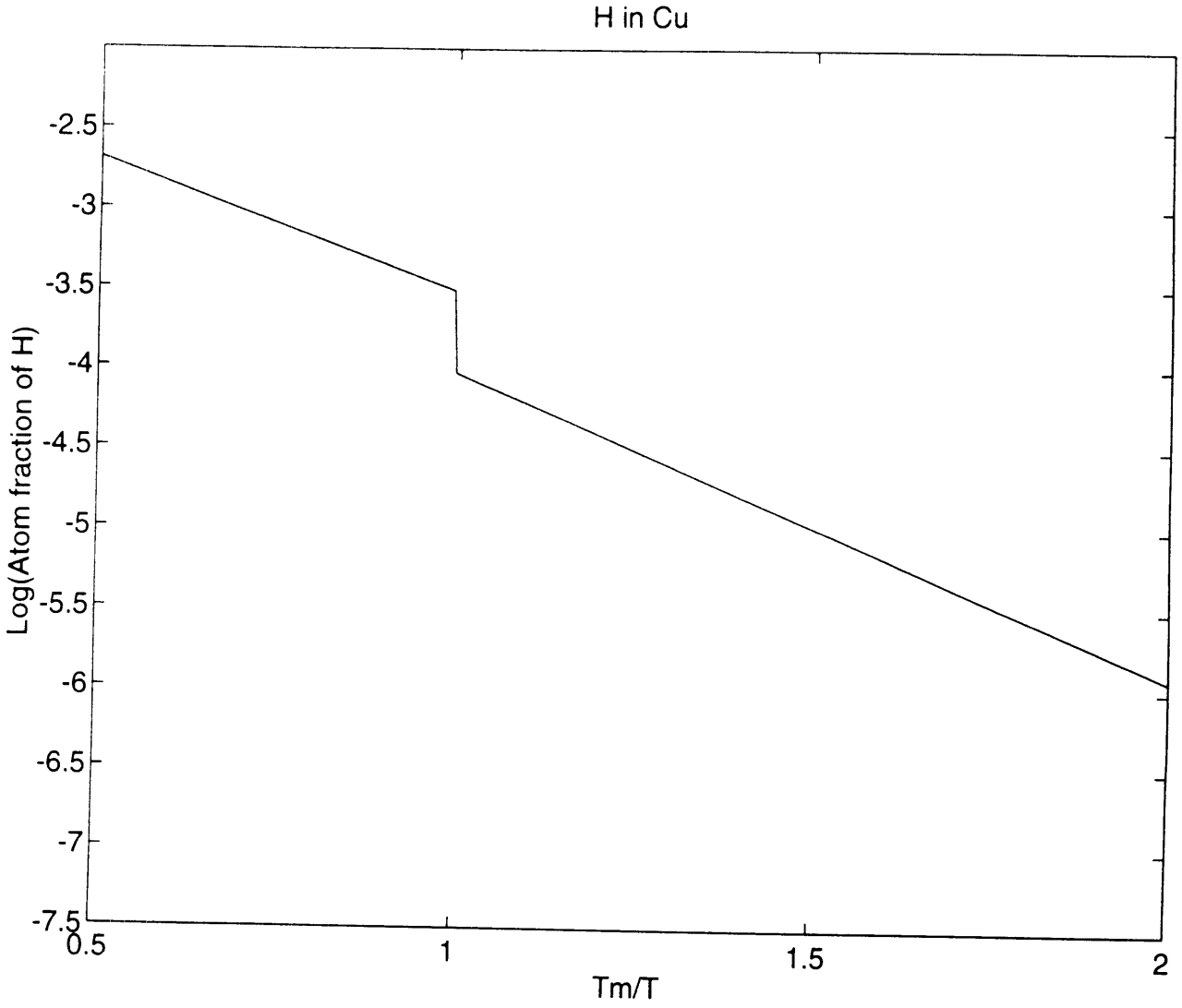

Figure 2.5 Solubility of hydrogen in Cu (P_{H2} = 1 atm)

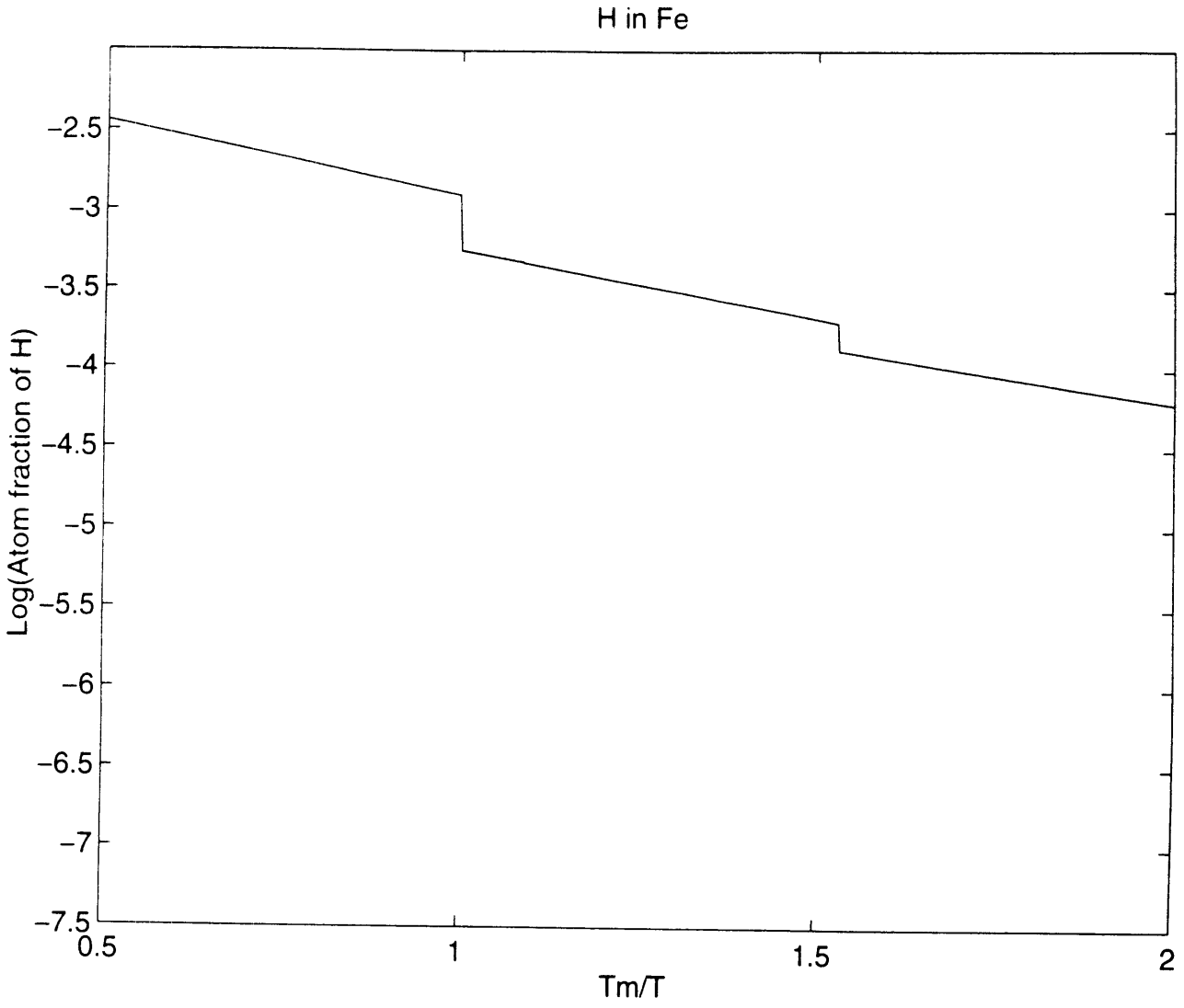

Figure 2.6 Solubility of hydrogen in Fe (P_{H2} = 1 atm)

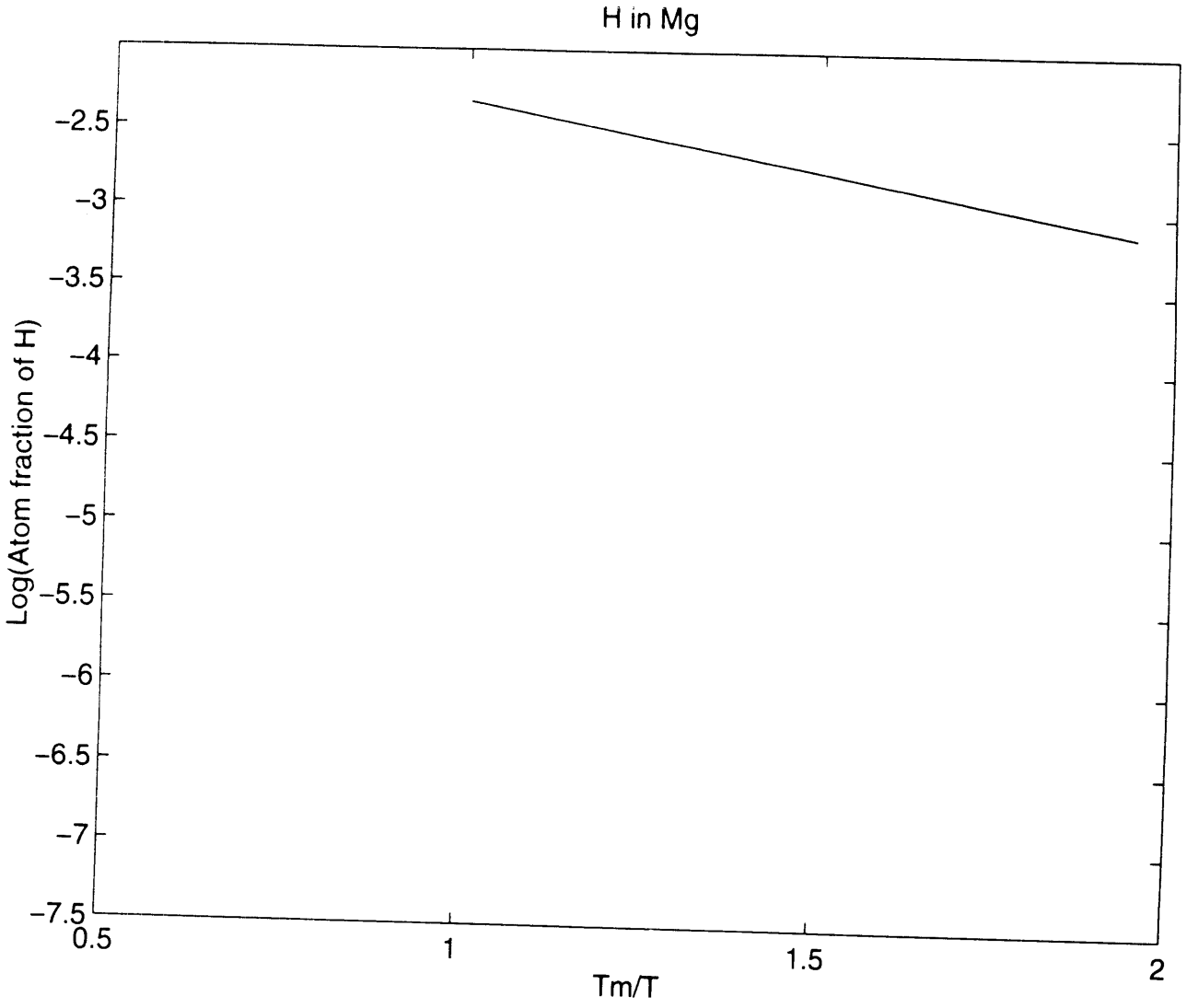

Figure 2.7 Solubility of hydrogen in Mg (P_{H2} = 1 atm)

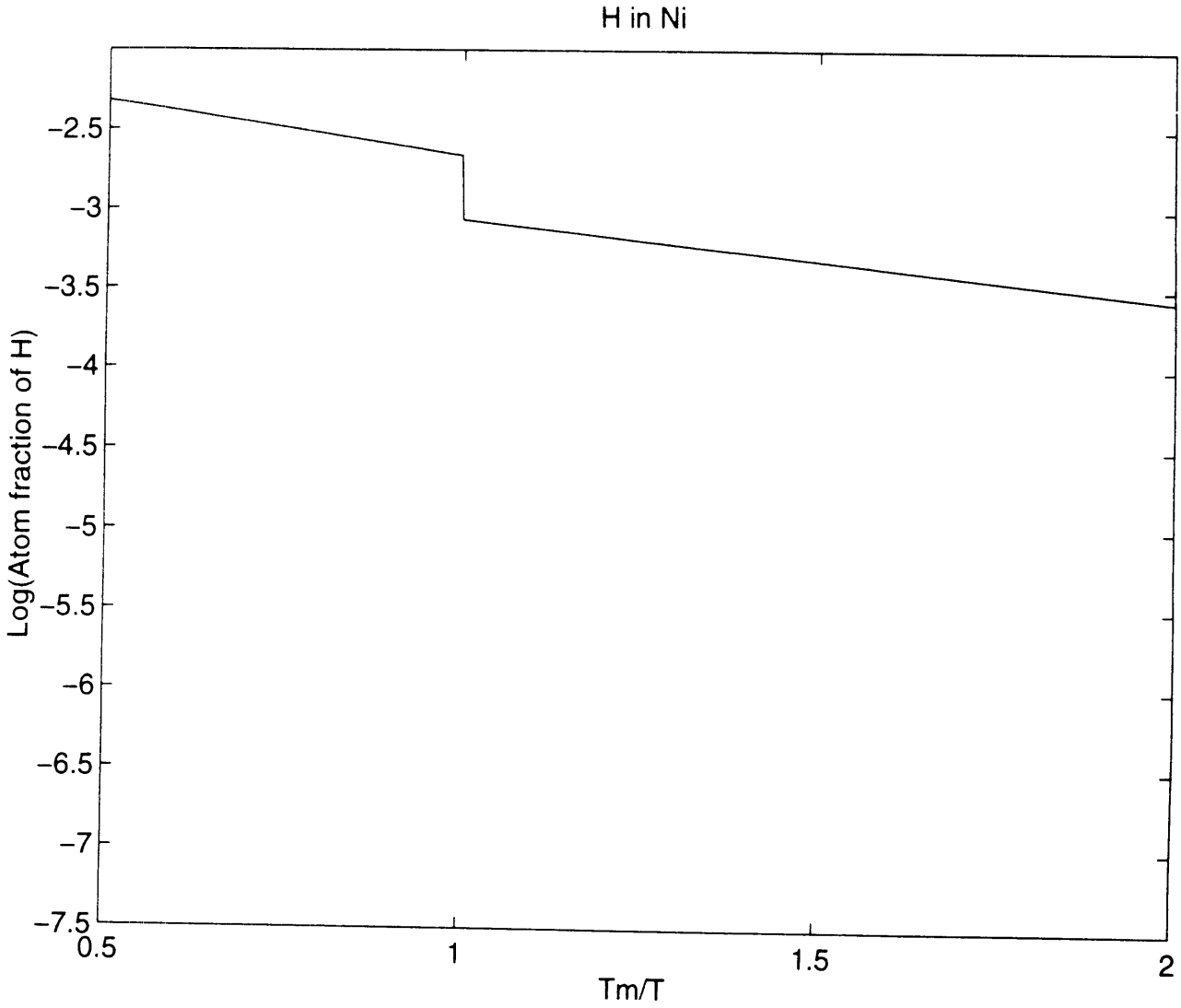

Figure 2.8 Solubility of hydrogen in Ni (P_{H2} = 1 atm)

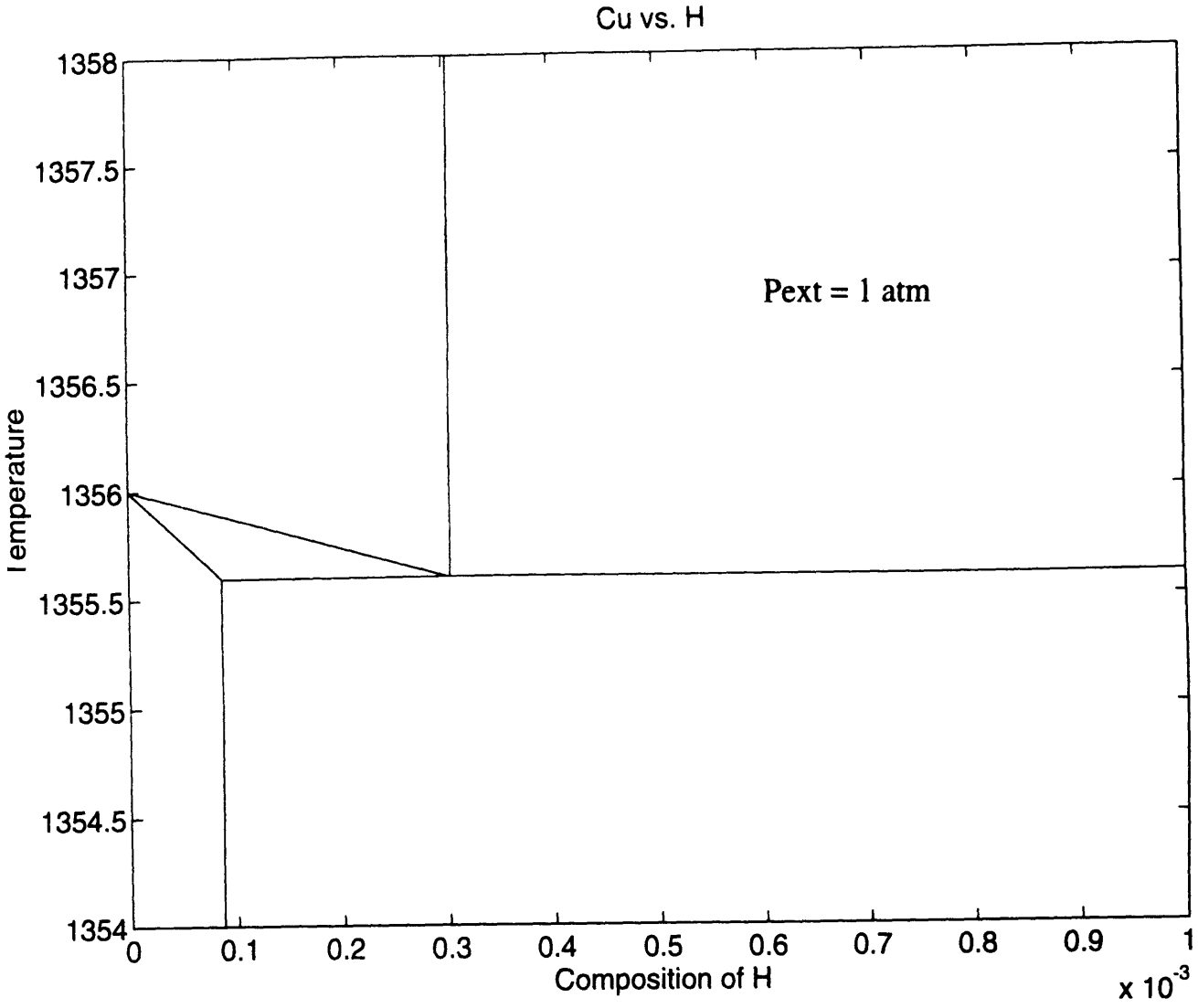

Figure 2.9 The Cu-rich portion of the Cu-H phase diagram (Pext = 1 atm)

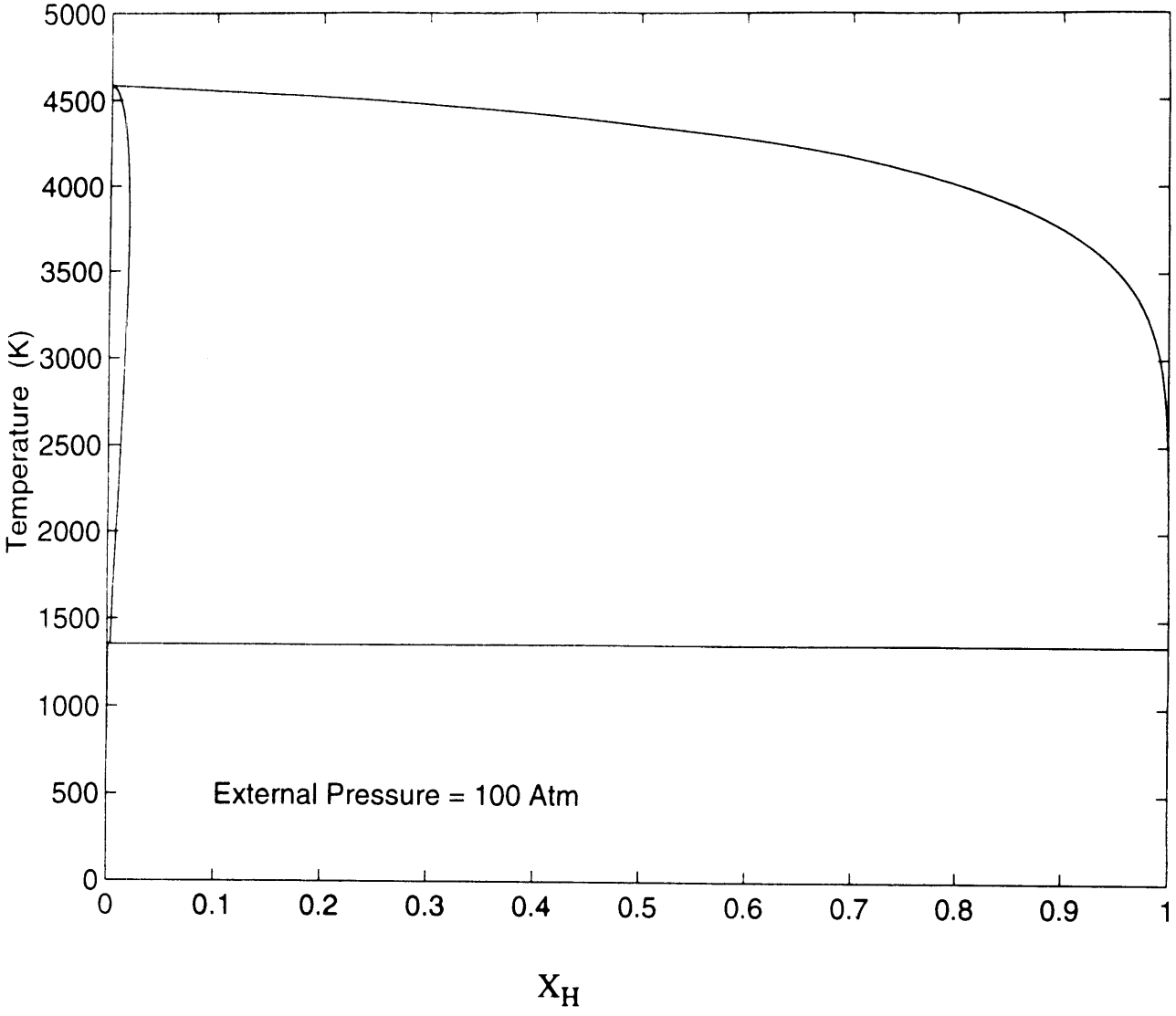

Figure 2.10 The phase diagram of the Cu-H system (Pext = 100 atm)

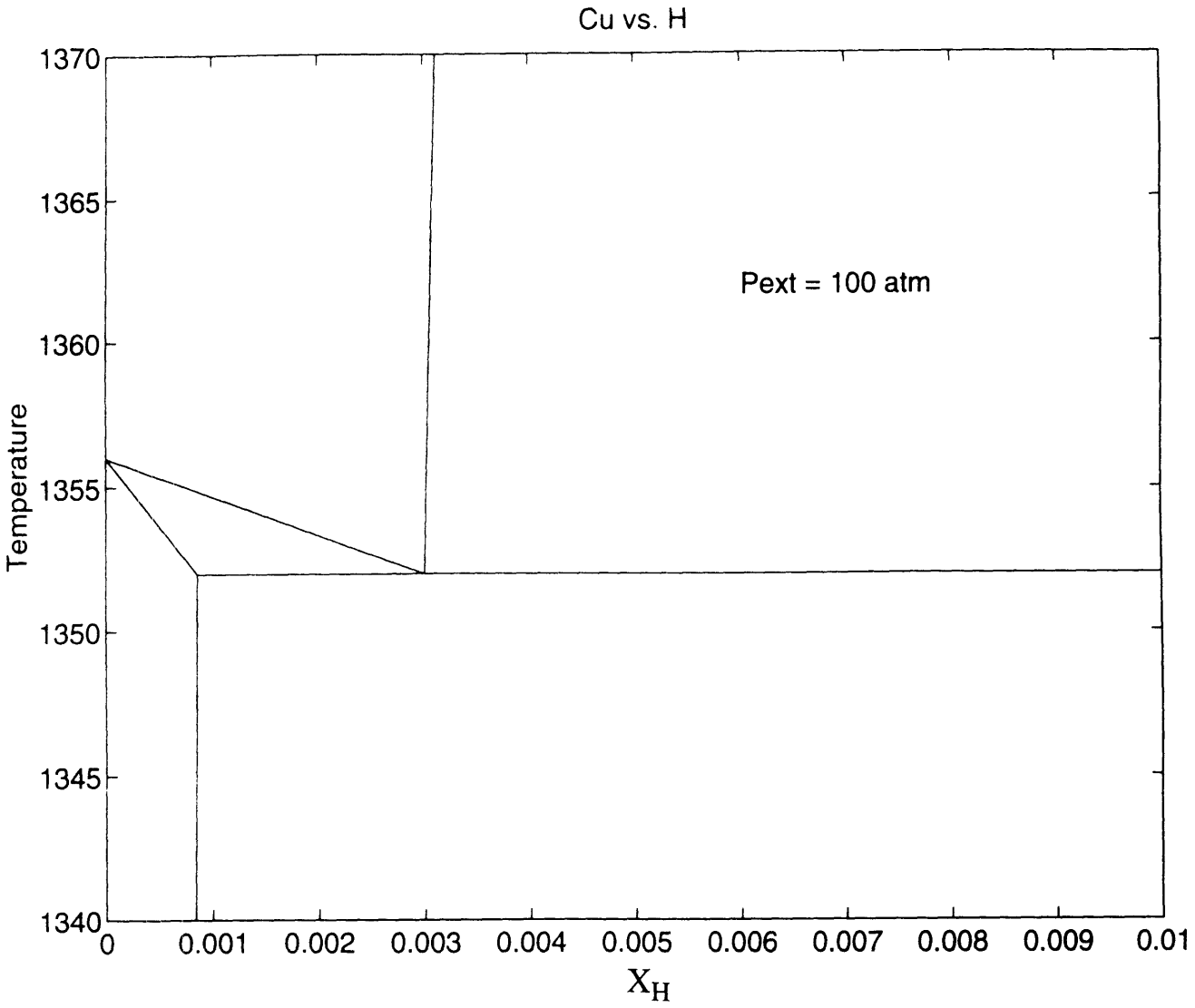

Figure 2.11 The Cu-rich portion of the Cu-H phase diagram (Pext = 100 atm)

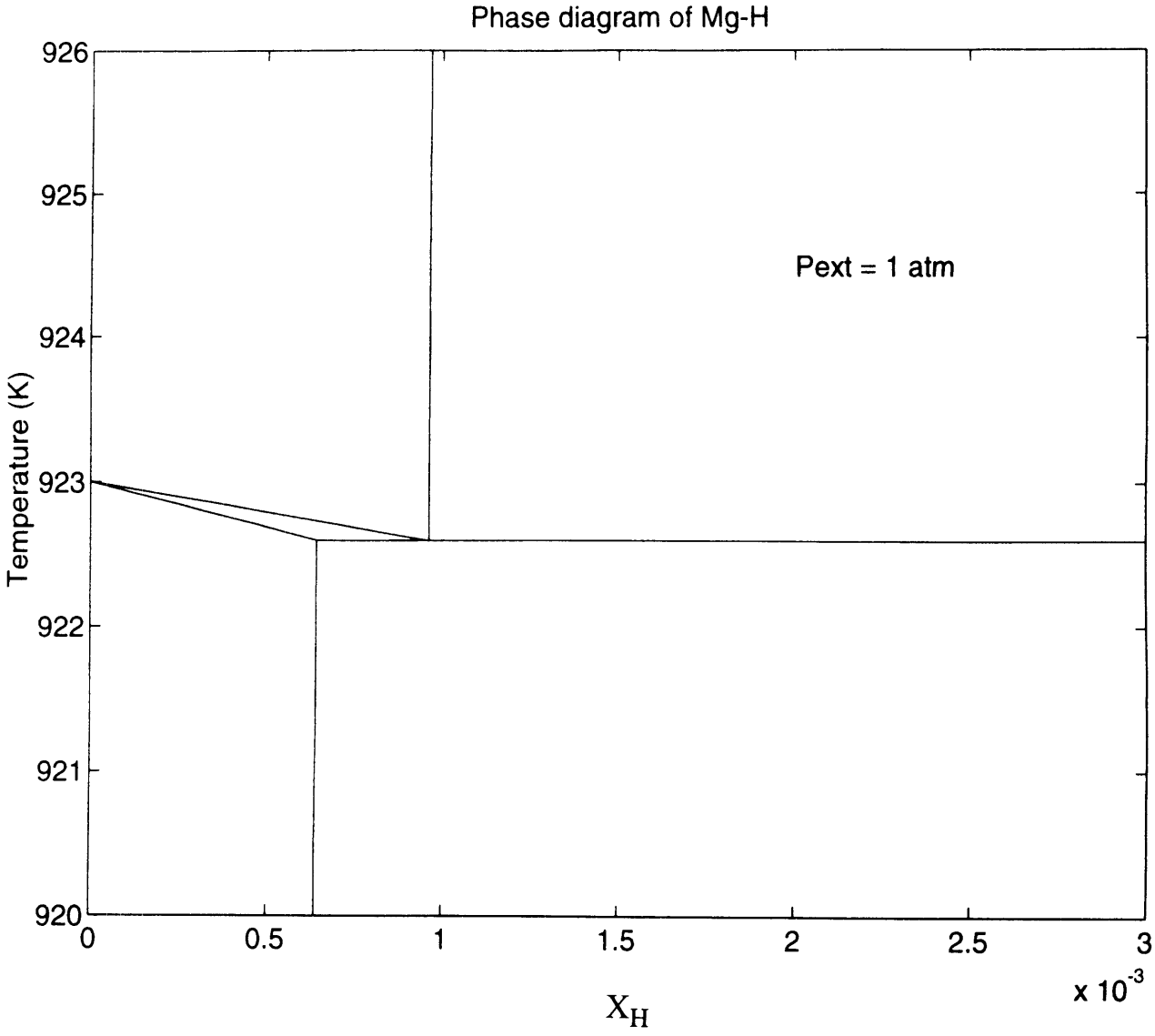

Figure 2.12 The Mg-rich portion of the Mg-H phase diagram (Pext = 1 atm)

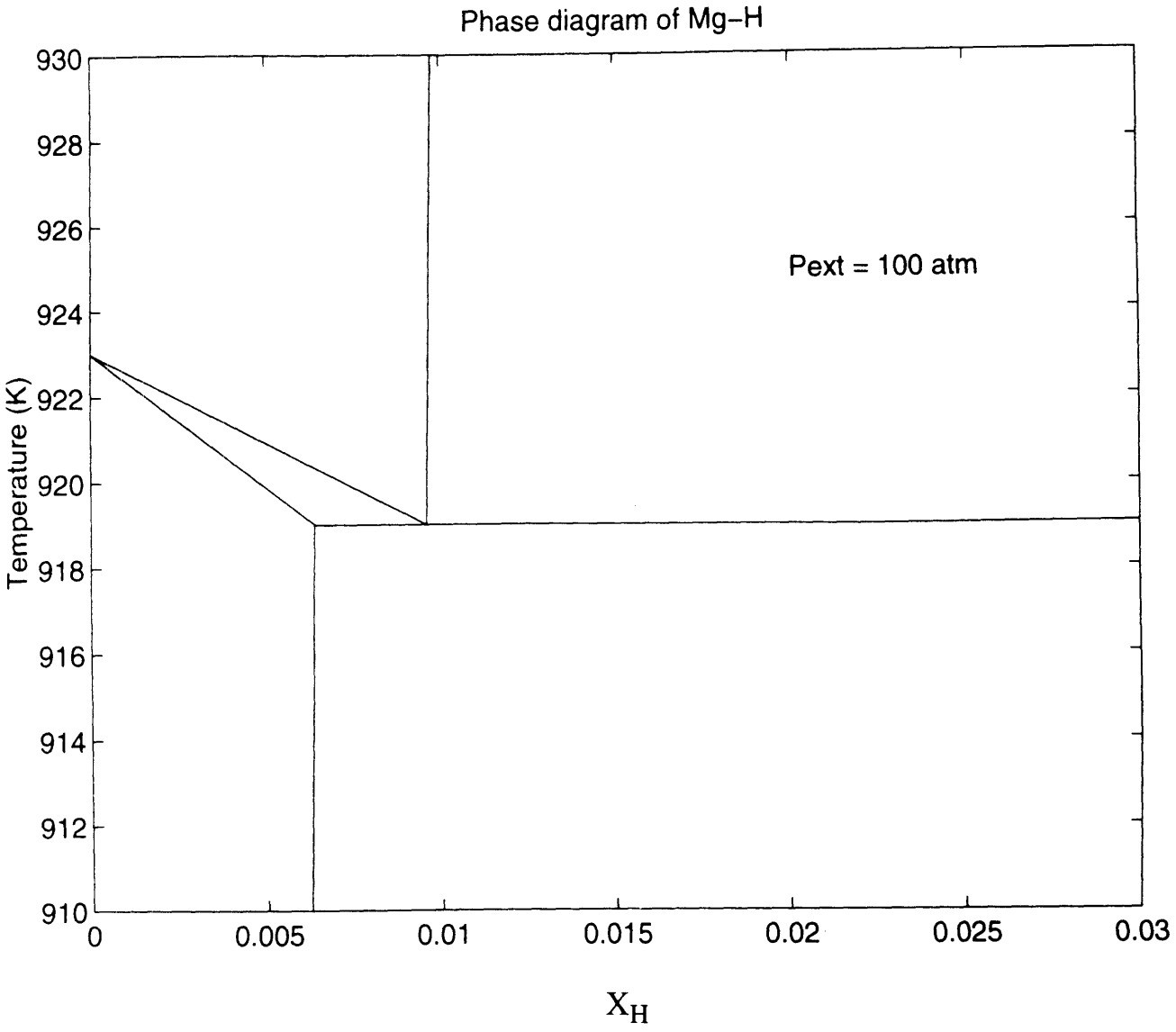

Figure 2.13 The Mg-rich portion of the Mg-H phase diagram(Pext = 100 atm)

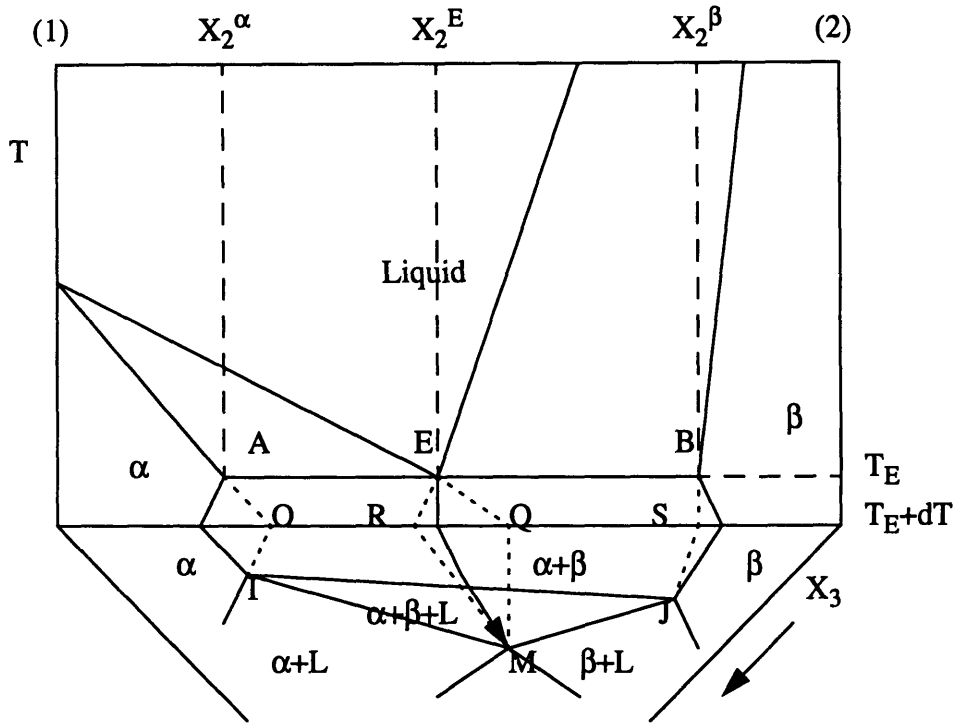

Figure 3.1 Graphical illustration of the effect of small additions of a third component on the eutectic temperature of a binary system.

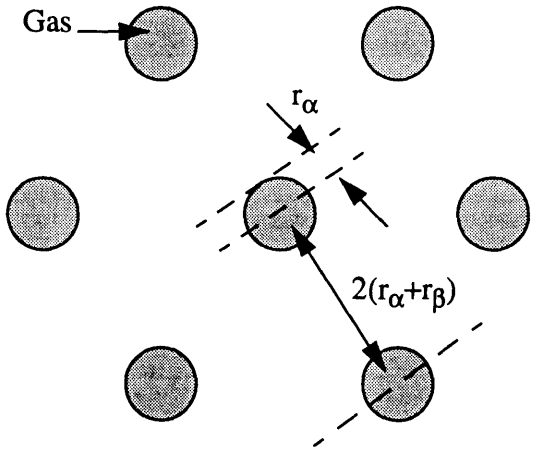

Figure 4.1 Schematic drawing of a rod structure viewed normal to the interface.

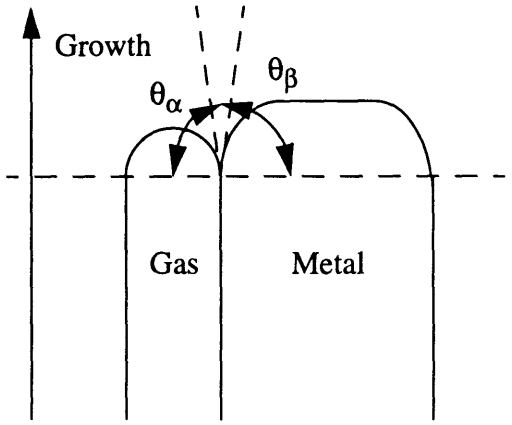

Figure 4.2 Schematic drawing of growing interface showing definition of θ.

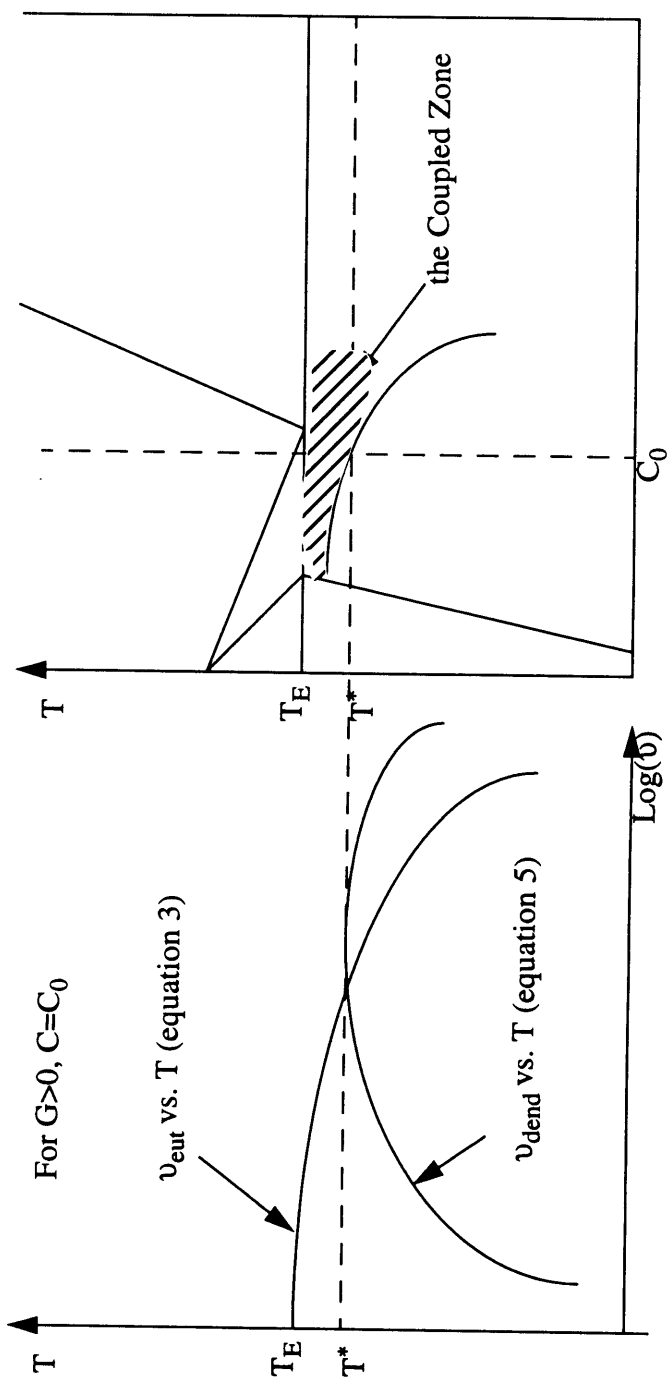

Figure 4.3 Comparing υ_{eut} with υ_{dend} to determine which growth is favorable.

Figure 4.4 The coupled zone resulted from comparing υ_{eut} with υ_{dend} .

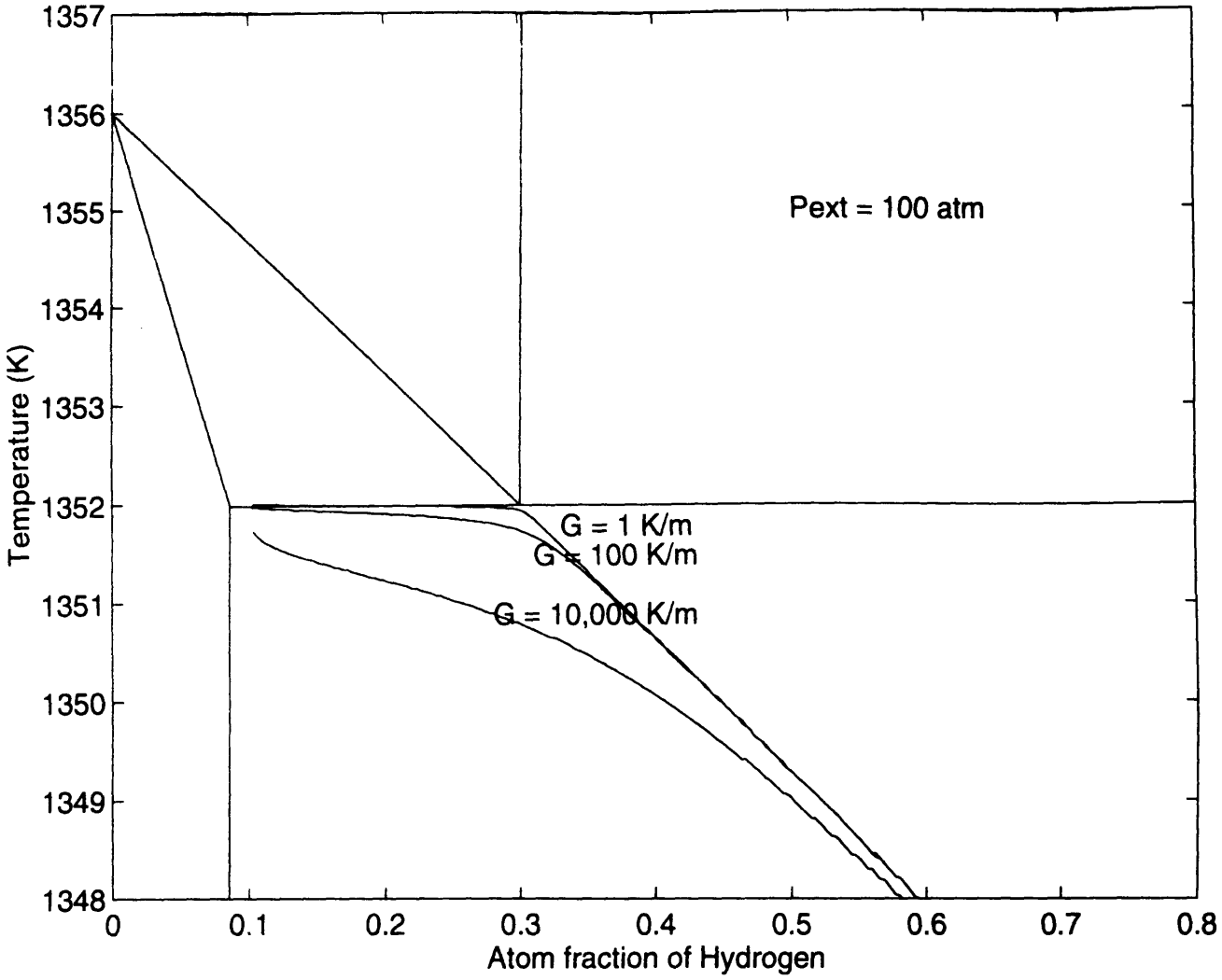

Figure 4.5 The Cu-H phase diagram with the coupled zone

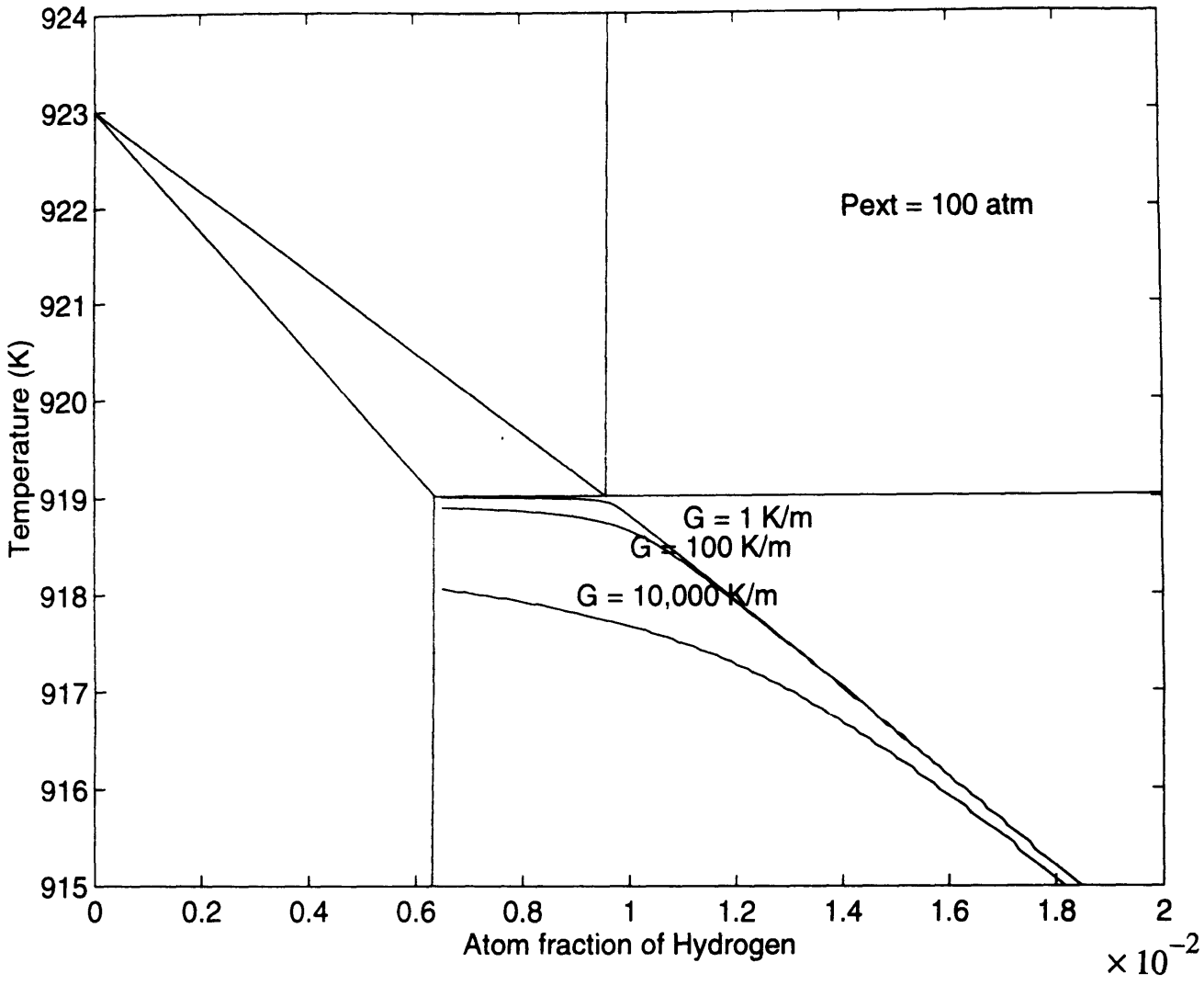

Figure 4.6 The Mg-H phase diagram with the coupled zone